

Article

[SBP]BF₄ Additive Stabilizing Zinc Anode by Simultaneously Regulating the Solvation Shell and Electrode Interface

Xingyun Zhang ^{1,2,†}, Kailimai Su ^{2,†}, Yue Hu ^{1,2}, Kaiyuan Xue ^{1,2}, Yan Wang ^{2,3}, Minmin Han ^{1,*} and Junwei Lang ^{2,3,*}

¹ College of Mechanical and Electrical Engineering, College of Materials Science and Engineering, Qingdao University, Qingdao 266071, China; 2021023612@qdu.edu.cn (X.Z.); huyue@qdu.edu.cn (Y.H.); 2021023631@qdu.edu.cn (K.X.)

² Laboratory of Clean Energy Chemistry and Materials, State Key Laboratory of Solid Lubrication, Lanzhou Institute of Chemical Physics, Chinese Academy of Sciences, Lanzhou 730000, China; suklm@licp.cas.cn (K.S.); wangyan@licp.cas.cn (Y.W.)

³ Shandong Laboratory of Advanced Materials and Green Manufacturing at Yantai, Yantai 264000, China

* Correspondence: hanminmin1@qdu.edu.cn (M.H.); jwlang@licp.cas.cn (J.L.)

† These authors contributed equally to this work.

Abstract: The zinc anode mainly faces technical problems such as short circuits caused by the growth of dendrite, low coulomb efficiency, and a short cycle life caused by side reactions, which impedes the rapid development of aqueous zinc-ion batteries (AZIBs). Herein, a common ionic liquid, 1,1-Spirobipyrrolidinium tetrafluoroborate ([SBP]BF₄), is selected as a new additive for pure ZnSO₄ electrolyte. It is found that this additive could regulate the solvation sheath of hydrated Zn²⁺ ions, promote the ionic mobility of Zn²⁺, homogenize the flux of Zn²⁺, avoid side reactions between the electrolyte and electrode, and inhibit the production of zinc dendrites by facilitating the establishment of an inorganic solid electrolyte interphase layer. With the 1% [SBP]BF₄-modified electrolyte, the Zn||Zn symmetric cell delivers an extended plating/stripping cycling life of 2000 h at 1 mA cm⁻², which is much higher than that of the cell without additives (330 h). As a proof of concept, the Zn||V₂O₅ battery using the [SBP]BF₄ additive shows excellent cycling stability, maintaining its specific capacity at 97 mAh g⁻¹ after 2000 cycles at 5 A g⁻¹, which is much greater than the 46 mAh g⁻¹ capacity of the non-additive battery. This study offers zinc anode stabilization through high-efficiency electrolyte engineering.

Keywords: aqueous zinc-ion batteries; ionic liquids; electrolyte; additive; zinc anode



Citation: Zhang, X.; Su, K.; Hu, Y.; Xue, K.; Wang, Y.; Han, M.; Lang, J. [SBP]BF₄ Additive Stabilizing Zinc Anode by Simultaneously Regulating the Solvation Shell and Electrode Interface. *Batteries* **2024**, *10*, 102. <https://doi.org/10.3390/batteries10030102>

Academic Editor: Atsushi Nagai

Received: 9 February 2024

Revised: 4 March 2024

Accepted: 8 March 2024

Published: 14 March 2024



Copyright: © 2024 by the authors. Licensee MDPI, Basel, Switzerland. This article is an open access article distributed under the terms and conditions of the Creative Commons Attribution (CC BY) license (<https://creativecommons.org/licenses/by/4.0/>).

1. Introduction

Due to the escalating severity of energy crises and environmental pollution caused by human technological progress and industrialization, the advancement of renewable power conversion/storage technologies has been a focus point and hot topic in the area of power storage [1,2]. Considering their elevated theoretical specific capacity (820 mAh g⁻¹), low redox voltage (−0.76 V vs. SHE), and abundant resources (three times that of lithium metal) of the zinc metal, as well as the cost-effectiveness, high safety, and high ionic conductivity of water-based electrolytes, aqueous zinc-ion batteries (AZIBs) have significant application value and prospects in areas ranging from mobile electronics and electric automobiles to the industrial sector [3,4]. Typically, AZIBs utilize manganese-based materials with large tunnel structures or vanadium-based layered materials as the cathode, with zinc alloys serving as the anode and normal or mildly acidic water-based compounds like ZnSO₄, ZnCl₂, and Zn(NO₃)₂ serving as the electrolyte [5]. At present, there are numerous challenges in the cathode, anode, and electrolyte aspects of AZIBs, and relevant research is in the transitional stage from scientific research to commercialization [6–8].

The zinc anode faces the main technical problems such as short circuits caused by the growth of dendrite, low coulomb efficiency, and a short cycle life caused by side reactions [9]. Among them, zinc dendrite growth is associated with the uneven deposition and solvation of zinc ions, while the side reactions are corrosion, hydrogen evolution, and obturation of the zinc anode [10]. Therefore, ensuring the reliability of the zinc anode is essential to promoting the practical application of AZIBs. It is not difficult to find that all the reactions occurring at the zinc anode in AZIBs involve strong interactions between Zn^{2+} and H_2O molecules. Firstly, the $Zn(H_2O)_6^{2+}$ solvated structure has a high energy barrier, resulting in difficult desolvation, high charge transfer resistance, and slow kinetics during charge and discharge. Secondly, $[Zn(H_2O)_6]^{2+}$ can provide a large number of active H_2O molecules on the interface of the zinc anode, thus causing various side reactions [11,12]. Thirdly, the zinc anode cannot easily form the solid electrolyte interface (SEI) film in an aquatic environment, and a bare zinc anode is prone to side reactions including erosion and hydrogen evolution. Thus, stabilizing the zinc anode requires mitigation of the solvation effect of Zn^{2+} with water and suppression of the activity of water molecules on the anode surface [13].

Researchers have adopted several strategies to increase the stabilization of the zinc anode, including (1) optimizing the electrode structure, (2) constructing functional interfacial layers on the zinc electrode skin, (3) optimizing the separator, and (4) adjusting the composition and concentration of the electrolyte or introducing additives [14–16]. However, the first three methods require a significant amount of time and involve high process costs [17]. High-concentration electrolytes also face challenges such as high cost, limited conductivity, and low-temperature salt precipitation. Introducing additives into electrolytes can directly optimize the solvation structure of Zn^{2+} , regulate the local current distribution, and improve the electrode/electrolyte interface properties [18]. In comparison, the introduction of additives is the simplest and most direct method for stabilizing the zinc anode and is compatible with existing battery manufacturing processes.

Electrolyte additives can be categorized as ionic additives (Na^+ , Mg^{2+} , Mn^{3+} , etc.), inorganic additives (oxides and inorganic acids), organic additives (small molecules, polymers, ionic liquids, etc.), and metal additives (lead and tin). Ionic additives containing heavy metals can cause environmental and electrolyte side reaction issues [19,20]. Inorganic and metal additives have received less research attention due to their limited solubility. Organic additives have been a popular topic as they can optimize the solvation structure of zinc ions, regulate uniform nucleation, induce epitaxial deposition, and even produce SEI films *in situ* [21]. They can also lessen the movement of water and zinc ions by creating hydrogen bonds with water molecules, thereby mitigating water-related side reactions. However, common organic additives have safety hazards such as flammability and toxicity [22]. Consequently, there is an urgent to explore new excellent performance additives that are highly stable, have a wide voltage window, are safe, and have low flammability.

Ionic liquids (ILs) consist of asymmetric organic cations and organic/inorganic anions, which have special characteristics such as a low melting point, good thermal and chemical stability, strong ionic conductivity, a broad electrochemical window, non-volatility, and non-combustibility and have been widely applied in energy storage batteries, metal deposition, organic synthesis, and other fields [23]. In terms of non-aqueous zinc-based batteries, ILs can be used alone as the electrolyte (EMI-DCA [24]) or as the solvent for zinc salt (EMImOTf [25]), and the resulting Zn//graphite battery showed no signs of dendrites or short circuits after hundreds of cycles. In the area of aqueous alkaline zinc batteries, adding a small amount of IL (EMI-DCA [24]) to the KOH electrolyte can improve the secondary nucleation process of zinc, prevent uneven zinc deposition, and inhibit dendrite formation. As for AZIBs, only EMIES [26], [Ch]OAC [27], [BMIM]OTf [28], Me3EtNOTF [29], DES [30], and PIL [31] have been reportedly applied as electrolyte additives, with related work only providing preliminary verification of their feasibility and excellent effects. In summary, other high-performance IL additives need to be screened to provide experimental data for the subsequent design of ideal IL additives with multiple functions such as

stabilizing the zinc anode, increasing the voltage window, and improving low-temperature performance [32].

In this paper, a common IL, $[SBP]BF_4$, was chosen as a novel addition to pure $ZnSO_4$ electrolyte, and its impact on the stability of the zinc anode and the performance of the whole battery was studied systematically [33,34]. In order to avoid side reactions between the electrolyte and electrode, it is discovered that the $[SBP]BF_4$ is preferentially adsorbed on the zinc anode and facilitates the creation of an inorganic SEI layer. On the other hand, the solvation sheath of hydrated Zn^{2+} ions may be controlled by the $[SBP]BF_4$, promote the ionic mobility of Zn^{2+} , homogenize the flux of Zn^{2+} , and thereby inhibit the formation of zinc dendrites. The findings of the experiment demonstrated that a minimal concentration of $[SBP]BF_4$ (1%) may effectively prevent the production of zinc dendrites and produce uniform zinc deposition. Consequently, the zinc anode delivered an extended plating/stripping cycling life of 2000 h in the $Zn||Zn$ symmetric cell with additive at 1 mA cm^{-2} , which is much higher than that of the cell without additives (where the life was only 330 h). Due to the critical dual functions originating from $[SBP]BF_4$, with 2000 cycles at 5 A g^{-1} , the $Zn V_2O_5$ battery maintained its specific capacity of 97 mAh g^{-1} , which is significantly higher than the non-additive battery's 46 mAh g^{-1} capacity; this indicates outstanding cycling stability.

2. Experimental Section

2.1. Materials

The following chemicals were procured from various suppliers: Pyrrolidine, 1,4-dibromobutane, and ammonium fluoroborate (NH_4BF_4) were acquired from Shanghai Macklin Chemical Co., Ltd., Shanghai, China. Potassium carbonate (K_2CO_3) and acetonitrile (ACN) were sourced from Sinopharm Chemical Reagents Co., Ltd., Shanghai, China. Vanadium pentoxide nanosheets were purchased from the same company. Zinc sulfate monohydrate ($ZnSO_4 \cdot H_2O$, AR) was obtained from Aladdin Reagent, Shanghai, China. Acetylene black was procured from Sinopharm Chemical Reagents Co., Ltd., China. Polyvinylidene fluoride (PVDF) was acquired from Sinopharm Chemical Reagents Co., Ltd., China. Finally, 1-methyl-2-pyrrolidone (NMP) was purchased from Sinopharm Chemical Reagents Co., Ltd., China.

2.2. Preparation of $[SBP]BF_4$

Pyrrolidine (1.1 mol, 78.2 g) was combined with 1,4-dichlorobutane (1.1 mol, 139.7 g) and potassium carbonate (2.1 mol, 290 g) in acetonitrile (ACN, 1.5 L). The resultant mixture was stirred under reflux at $60\text{ }^\circ C$ for 20 h. Upon cooling, the mixture was filtered and the filtrate was subjected to vacuum drying to yield 170 g of a crude chlorinate salt. This crude product was then treated with 50% hydrofluoroboric acid (HBF_4 , 0.9 mol, 155 g) and ethanol at room temperature for 20 h to facilitate an ion exchange reaction, converting the chloride salt to a BF_4 salt. The reaction mixture was evaporated, and the residual salt was purified through multiple recrystallization steps using ethanol. Following recrystallization, the product was thoroughly dried under vacuum at $90\text{ }^\circ C$ to afford the ionic liquid additive $[SBP]BF_4$ in a suitable white crystalline form with a purity of 99.99%.

2.3. The Chemical Structure Characterization of $[SBP]BF_4$

The synthesized $[SBP]BF_4$ sample was dissolved in a dimethyl sulfoxide (DMSO) solution, and the anions and cations of the sample were analyzed using nuclear magnetic resonance spectroscopy (NMR) (Figures S2 and S3). The 1H NMR (400 MHz, DMSO- d_6) spectrum is depicted in the figure, with an integral ratio of δ 3.41 (s, 1H) to δ 2.03 (s, 1H) protons at 1:1. The ^{19}F NMR (376 MHz, DMSO- d_6) spectrum showed an integral of δ -148.62 (d, $J = 20.4\text{ Hz}$) proton at 1. The presence of DMSO solvent and residual water was also confirmed at dw2.49 and dw3.33, respectively. In conclusion, the NMR data confirm that the synthesized sample was $[SBP]BF_4$.

2.4. Preparation of V_2O_5 Cathode

The synthesis of the V_2O_5 cathode was conducted following methods described in the existing literature [18]. Initially, a mixture of 70% V_2O_5 (0.21 g), 20% acetylene black (0.06 g), and 10% PVDF (0.03 g) was combined in a mortar. Then, 5 mL of NMP solvent was added and stirred manually for 3 h to obtain a slurry with a viscosity of 6000 mPa·S. Subsequently, the electrode slurry was uniformly coated onto graphite paper. The coated electrode was then subjected to vacuum drying at 50 °C for 12 h to facilitate solvent removal.

2.5. Materials Characterization

The crystal structure and phase of the material were ascertained using X-ray diffraction (XRD, GBC MMA diffractometer, Super-Dimensional Technology Co., Ltd., Taiwan, China). Fourier transform infrared spectroscopy (FTIR, Nexus 870, Thermo Fisher Nicolet, Waltham, MA, USA) and Raman spectroscopy (DXR3xi, Thermo Scientific, Waltham, MA, USA) were employed to investigate changes in functional groups and the sample's molecular structure. The elemental composition and atomic valence were analyzed using X-ray photoelectron spectroscopy (XPS, ESCALAB 250, Thermal Power Corporation, Waltham, MA, USA). Field emission scanning electron microscopy (FE-SEM, Hitachi Regulus 8100, Hitachi, Tokyo, Japan) and transmission electron microscopy (TEM, JEM-2100FEG, Nippon Electronics Co., Tokyo, Japan) were utilized to study the material's morphology.

2.6. Electrochemical Tests

The electrochemical properties of the $Zn \parallel Zn$ symmetric battery, $Zn \parallel Cu$ asymmetric battery, and $Zn \parallel V_2O_5$ full battery were studied by assembling the CR2032 button battery. Zinc-zinc symmetric batteries were prepared by using $ZnSO_4$ aqueous solution with and without $[SBP]BF_4$ additive as an electrolyte, glass fiber as a separator, and two identical zinc foils as positive and negative electrodes. The stability of the zinc anode was evaluated at a current density of 1 $mA\ cm^{-2}$ using the LAND battery test system (CT3002A Wuhan, China). The $Zn \parallel Cu$ battery, which employs Zn foil as the negative electrode and Cu foil as the positive electrode, underwent a prolonged cycle test at a capacity of 0.5 $mAh\ cm^{-2}$ at 2 $mA\ cm^{-2}$. The CHI660E electrochemical workstation conducted cyclic voltammetry (CV) testing at a scan rate of 1 $m\ Vs^{-1}$, chronoamperometry (CA) testing at an overpotential of 10 mV for 600 s, and electrochemical impedance spectroscopy (EIS) testing within the frequency range of 0.01~105 Hz. The $Zn \parallel V_2O_5$ full cell, assembled with a Zn anode and V_2O_5 cathode, was subjected to CV, cycle, and rate tests at different current densities of 0.2~1.6 V and 0.5~1.6 V. These evaluations confirmed the practical applicability of the $[SBP]BF_4$ additive.

3. Result and Discussion

3.1. Structural Characterization Analysis

It is clear from Figure 1a that the initial stage of Zn deposition is usually uneven and is mainly caused by the recognized “tip effect”, and finally, obvious Zn dendrites are formed [35]. Simultaneously, the Zn anode/electrolyte contact experiences the development of H_2 and the formation of by-products, both of which invariably result in fast capacity loss [30]. To solve these problems, we proposed using an IL named $[SBP]BF_4$ as a functional electrolyte additive, which not only ensures the uniform deposition of Zn but also avoids the occurrence of adverse reactions. To verify these functions, AZIBs were constructed by incorporating different amounts of $[SBP]BF_4$ into 22wt% $ZnSO_4$ aqueous solution.

As shown in Figure 2a, by using the X-ray diffraction (XRD) technique, the composition of chemicals on the surface of zinc anodes after 70 cycles was examined. Apart from significant zinc deposition on the zinc anode surface during cycling in the absence of the $[SBP]BF_4$ additive, diffraction peaks equivalent to the $Zn_4SO_4(OH)_6 \cdot 4H_2O$ by-product were also seen at 8.3° and 12.1° [31]. This is because the hydrogen evolution side reaction produced a large amount of OH^- , which formed these by-products by combining with Zn^{2+} , SO_4^{2-} , and H_2O in the electrolyte. However, no by-product peak was observed on

the surface of the zinc electrode after cycling in the electrolyte with $[SBP]BF_4$ additives, indicating that the additive inhibited the generation of by-products. Furthermore, we found that the addition of $[SBP]BF_4$ was advantageous for weakening the solvation between Zn^{2+} and water. The FTIR spectra of pure $ZnSO_4$ electrolytes and electrolytes containing varying concentrations (0.5wt%, 1wt%, and 2wt%) of $[SBP]BF_4$ were compared in Figure 2b–d. The O-H stretching vibration peak of water at 3000–4000 cm^{-1} gradually moved to higher wavenumbers with the increase in additive content, which indicated that SBP^+ cations were beneficial for weakening the interaction between water molecules and Zn^{2+} cations. The vibration stretching peak representing SO_4^{2-} at 900–1200 cm^{-1} also shows a blue shift [32], indicating that the addition of additives damaged the electrostatic coupling between Zn^{2+} and SO_4^{2-} , thereby weakening the binding around SO_4^{2-} [33]. In addition, by comparing Raman spectra of pure $ZnSO_4$ electrolyte and electrolytes with different $[SBP]BF_4$ content, it was thoroughly shown that the addition of $[SBP]BF_4$ can lower the activity of the water molecules in the electrolyte. As illustrated in Figure 2e,f, when the additive content increases, the shoulder peak at 3396 cm^{-1} in the Raman spectra gradually weakened and shifted to a higher wavenumber; this demonstrates how the interaction between $[SBP]BF_4$ and water molecules damaged the initial hydrogen bond network. In summary, Zn^{2+} solvation in water can be lessened by $[SBP]BF_4$ addition, which also accelerates the desolvation of hydrated zinc ions, achieves the homogenization of zinc ion flux, and inhibits the decomposition of water molecules, thereby suppressing dendrite growth and mitigating the occurrence of side reactions.

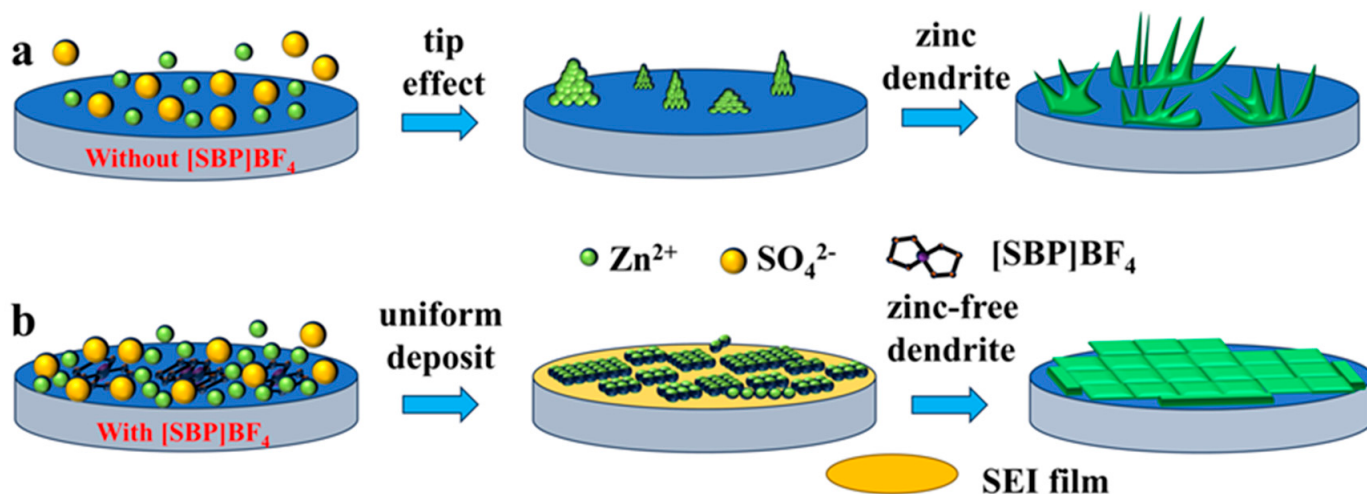


Figure 1. The schematic diagram of the Zn deposition process in the electrolyte (a) without and (b) with $[SBP]BF_4$ additive.

After 70 cycles, X-ray photoelectron spectroscopy (XPS) was used to characterize the Zn electrode both with and without Ar^+ deep sputtering; the results are displayed in Figure 3a,b. In the absence of $[SBP]BF_4$, C-C and O-C=O can be detected in the C1s spectra of both the zinc electrode surface (no Ar^+ sputtering) and the inner side (Ar^+ sputtering for 5 min), which may mainly be caused by the strong bonded glass fiber separator or CO_2 dissolved in the electrolyte from air [34]. After introducing $[SBP]BF_4$, in addition to the detection of O-C=O peaks related to inorganic $ZnCO_3$, organic components such as C-N, C-H, and C-C were also detected on the surface and inside of the zinc anode, indicating that $[SBP]BF_4$ molecules were adsorbed or decomposed. Analyzing the Zn2p spectra, in the absence of additives, only the loose structure formed by the unevenly distributed ZnO was detected on the surface and inside of the zinc. However, when $[SBP]BF_4$ is present, a large amount of $Zn(OH)_2$ and ZnO inorganic substances was detected both on the surface and inside of the zinc [35]. In addition, for the high-resolution F1 spectra, no F-containing inorganic zinc salt was detected regardless of the sputtering time when

there was no [SBP]BF₄. In stark contrast, when [SBP]BF₄ was added, inorganic ZnF₂ was found on the zinc anode surface, and the peak intensity of ZnF₂ escalated with an increase in Ar⁺ sputtering depth, suggesting that ZnF₂ not only resided on the surface but also intermingled with organic components embedded within the SEI layer. The existing literature confirms that inorganic constituents like Zn(OH)₂, ZnO, and ZnF₂ within the SEI layer have been proven to possess good Zn²⁺ conductivity and hydrophobicity. In summary, adding [SBP]BF₄ additives caused a thick material to develop, as well as a homogeneous SEI layer via organic/inorganic hybridization on the zinc electrode surface. This not only gives it robust toughness but also provides ample transport channels for electrolyte ions [36]. The SEI film not only keeps the aqueous solution and electrode from coming into direct contact, which reduces side reactions related to hydrogen evolution and corrosion, but it also makes it easier for Zn²⁺ to deposit evenly and inhibits the swift proliferation of zinc dendrites.

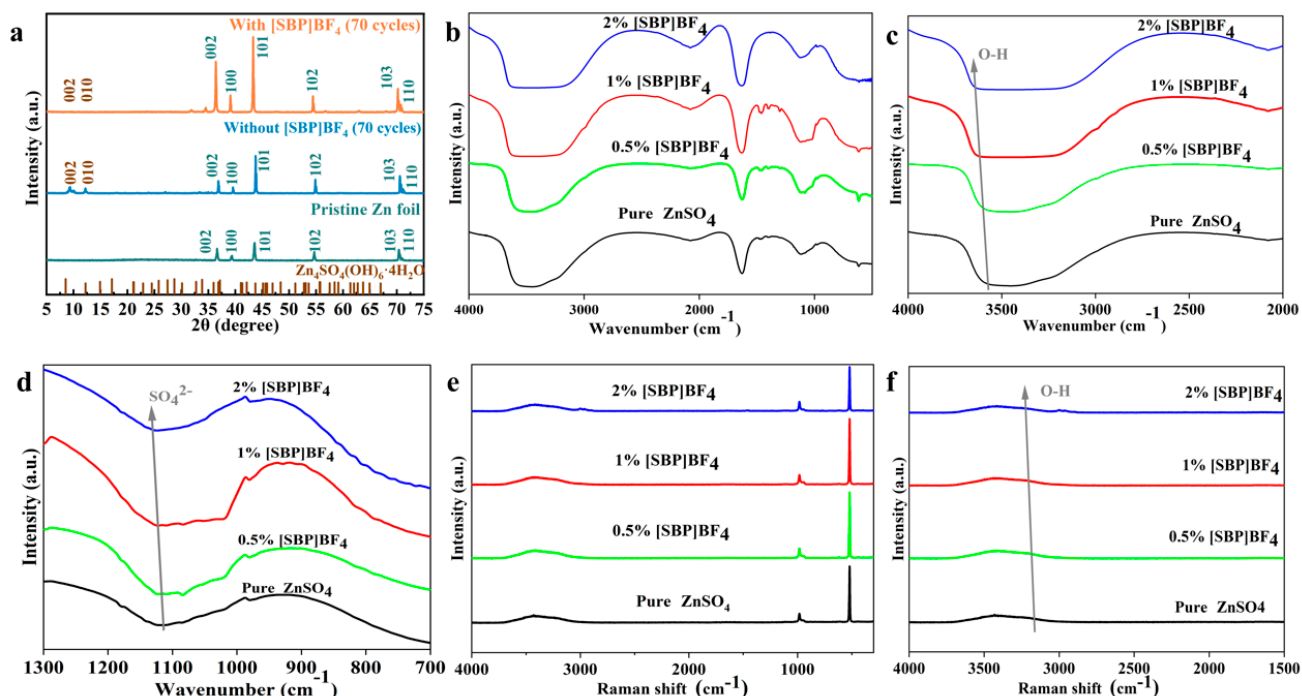


Figure 2. (a) XRD patterns of the original zinc foil and the zinc foil after 70 cycles in electrolytes with [SBP]BF₄ and without [SBP]BF₄. FTIR spectra (b–d) and Raman spectra (e,f) of electrolytes containing different proportions of [SBP]BF₄.

To see how the [SBP]BF₄ addition affected the formation of zinc dendrites, scanning electron microscopy (SEM) pictures (Figure 4a,b) were utilized. Without the addition of [SBP]BF₄, disordered and complex dendritic dendrites appeared on the surface of zinc foil, and there were many glass fibers around the dendrites. However, with the addition of additives, zinc foil's surface morphology underwent a dramatic alteration, dendritic development was suppressed, and a dense, homogenous planar structure developed [36]. The optical microscope images further verified that the consistent deposition of zinc ions on the zinc anode's surface was positively impacted by the addition of [SBP]BF₄. Figure 4c,d demonstrate this; many network dendrites appeared on the surface of the zinc sheet without the [SBP]BF₄ additive, resulting in an irregular and rough appearance. After adding [SBP]BF₄, there were no obvious dendrites on the surface of the zinc sheet, and the number of protrusions and dents was also reduced. This showed that the addition of [SBP]BF₄ effectively prevented the formation of unwanted side reactions and the development of zinc dendrites, producing a uniform and smooth zinc sheet surface. Atomic force microscopy (AFM) was used to characterize the three-dimensional profile and roughness of the zinc

anode surface in different states (Figure 4e–g). As can be seen from Figure 4g, the polished original zinc foil has a smooth surface with a height of about 94.7 nm. In the ZnSO_4 electrolyte without additives, Zn^{2+} primarily deposited on the protrusions on the surface of the zinc anode due to the uneven electric field [37]. Therefore, following 140 h of cycling in pure ZnSO_4 electrolyte, the surface of the zinc electrode becomes highly rough, with many zinc dendrites with a height of about 929.4 nm. In contrast, after cycling in the electrolyte containing $[\text{SBP}] \text{BF}_4$ for 140 h, the tip effect was weakened, the surface of the zinc foil remained relatively smooth and uniform, and the height was dropped to 537.5 nm. It can be seen that the $[\text{SBP}] \text{BF}_4$ additive can successfully stop zinc dendritic growth and has a positive effect on achieving a long cycle of the battery.

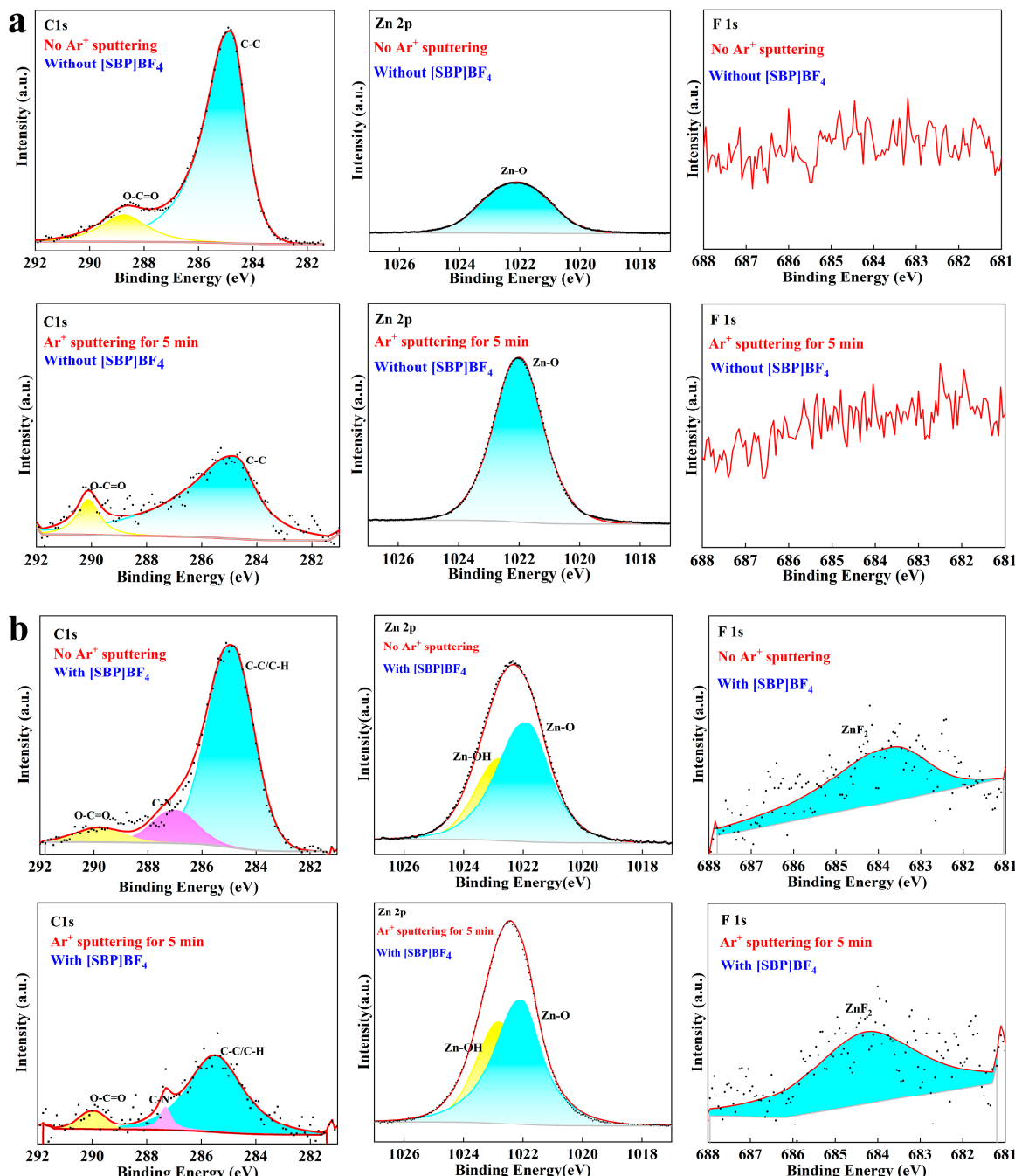


Figure 3. The XPS spectra of the Zn foils after 140 h cycles in (a) pure ZnSO_4 and (b) $\text{ZnSO}_4 + 1\text{wt}\%$ $[\text{SBP}] \text{BF}_4$ electrolytes.

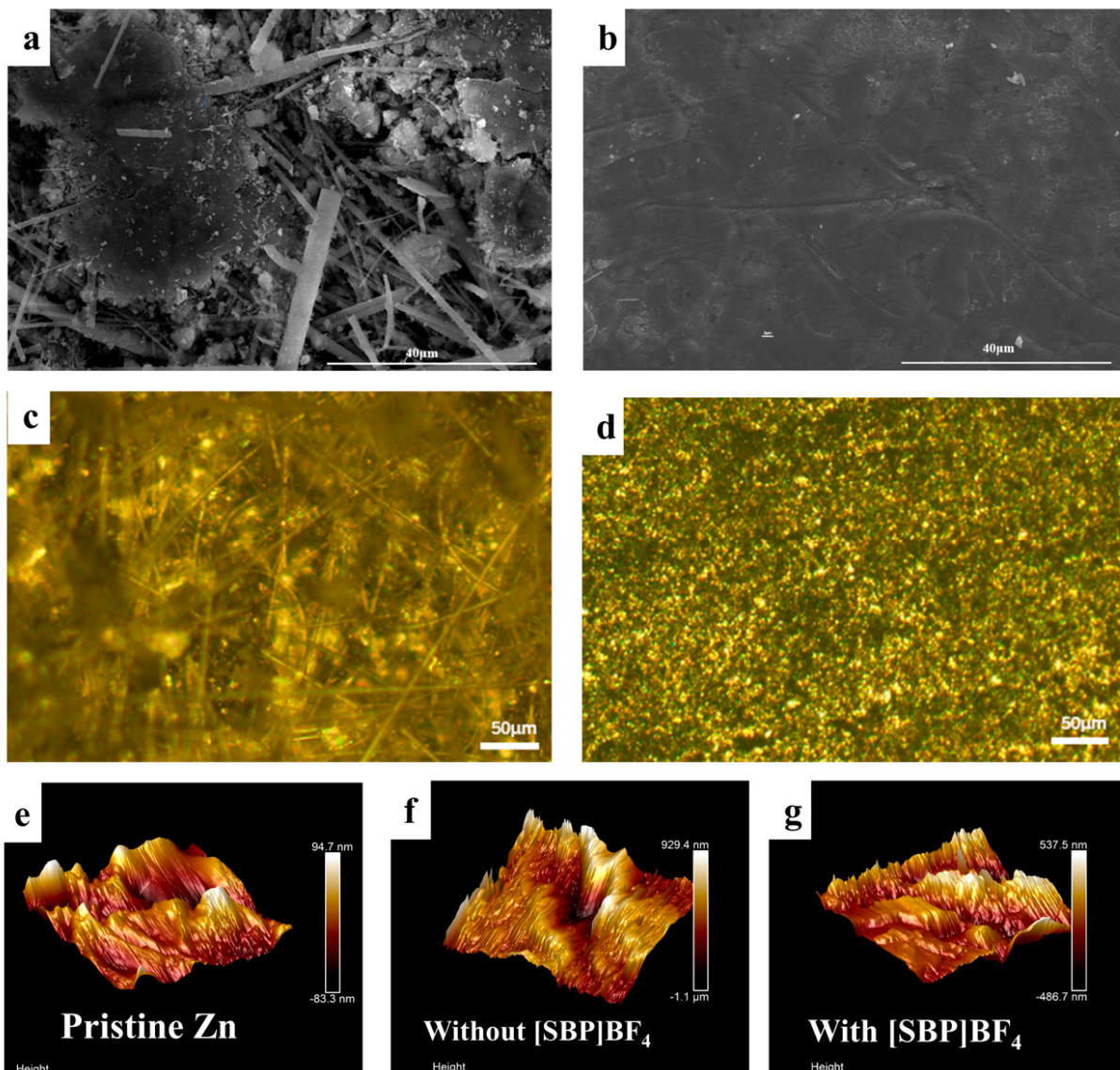


Figure 4. SEM images and optical microscope images of zinc electrode after 140 h cycling in (a,c) pure ZnSO_4 electrolyte and (b,d) electrolyte containing [SBP] BF_4 . AFM images of (e) the original Zn foil and (f,g) Zn foil after 140 h cycling in different electrolytes.

3.2. Electrochemical Measurement

To ascertain the impact of the [SBP] BF_4 additive on the electrochemical stability of the zinc anode, we assembled a three-electrode system (the working electrode and counter electrode are zinc, and the reference electrode is Ag/AgCl) with $\text{Zn} \parallel \text{Zn}$ symmetrical batteries and tested their electrochemical properties in detail. The corrosion activity of zinc anodes in batteries with and without additives was characterized by linear voltammetry, and the result is shown in Figure 5a. It can be observed that the Zn corrosion potential of the zinc anode in batteries with 1wt% [SBP] BF_4 and without the [SBP] BF_4 additive was -914 mV and -929 mV, respectively, indicating that the [SBP] BF_4 additive can prevent the corrosion of the Zn electrode to a certain extent by inhibiting hydrogen evolution reaction [38]. In addition, as shown in Figure S1, the cyclic voltammetry (CV) curves of $\text{Zn} \parallel \text{SS}$ (stainless steel) asymmetric batteries with and without the [SBP] BF_4 additive were obtained. The introduction of the [SBP] BF_4 additive increased the nucleation sites of the cell from 63 to 96 mV, which can reduce the radius of the Zn crystal nucleus and facilitate the formation of a compact, flat, and uniform layer of Zn [39]. Consequently, this prevented the growth of zinc dendrites.

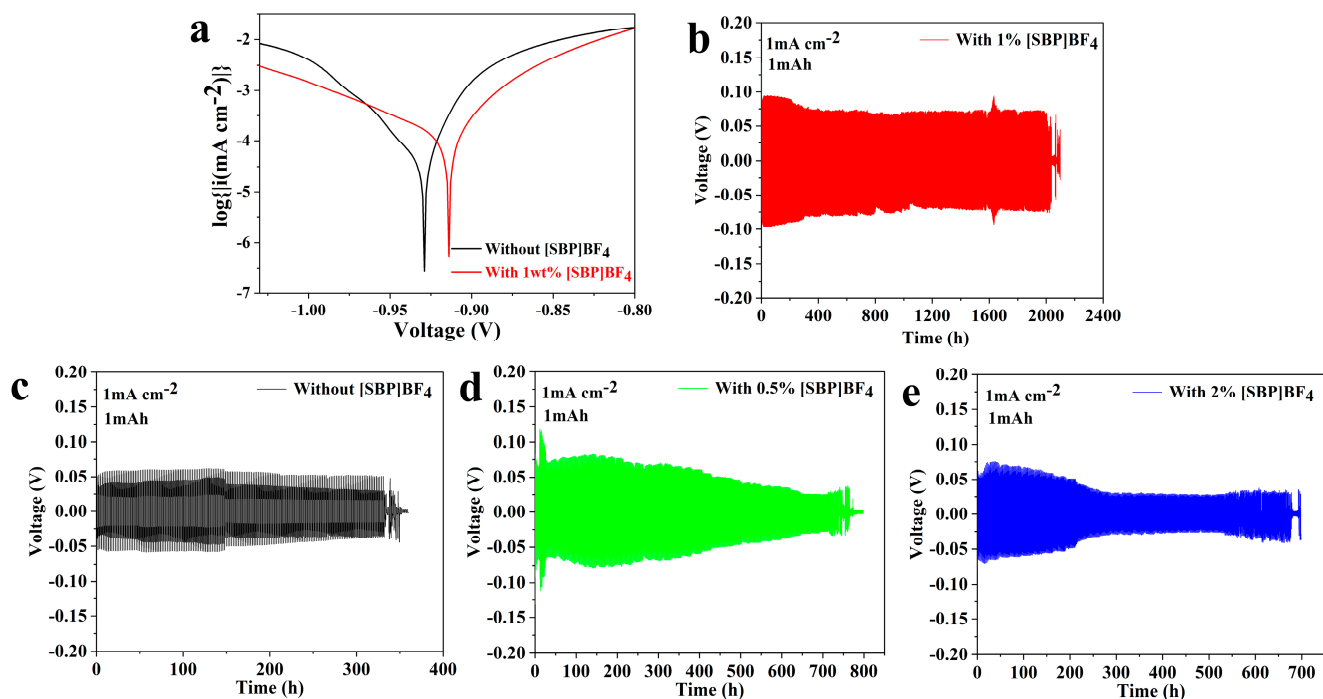


Figure 5. (a) The potentiodynamic polarization curves of the zinc anode in three-electrode system in electrolyte with 1wt% [SBP]BF₄ and without [SBP]BF₄. (b–e) The constant current charge and discharge cycle performance of Zn || Zn symmetrical battery using electrolytes with different proportions of [SBP]BF₄ additive at 1 mA cm^{-2} .

By evaluating the Zn || Zn symmetric battery's constant current charge–discharge curve, the Zn plating/stripping process on the Zn anode during long-term cycling may be examined. The results show that the batteries with different electrolytes exhibit different cycle life at a constant current density of 1 mA cm^{-2} and a cut-off capacity of 1 mAh cm^{-2} . As shown in Figure 5b–e, the battery using pure ZnSO₄ electrolyte was damaged after 330 h of cycling and therefore has a short life. After the addition of [SBP]BF₄ into the electrolyte at ratios of 0.5% and 2%, it was found that the battery life was prolonged, but the polarization voltage was unstable, and they failed after 670 h and 680 h, respectively. It was worth noting that when the content of [SBP]BF₄ is 1%, the resulting Zn || Zn battery exhibits a steady overpotential, and the cycle lifespan was up to 2000 h, which was significantly better than other batteries. It was proven that the [SBP]BF₄ additive can affect the nucleation site of Zn²⁺ and encourage consistent and steady zinc plating or stripping on the zinc anode, which may successfully avoid the occurrence of zinc dendrites [40].

To further demonstrate that the [SBP]BF₄ additive can improve the cycle stability of the zinc anode, Zn || Cu batteries were assembled and their electrochemical performance was tested. In the discharge process, the zinc stripped from the zinc anode in the battery will be deposited on the copper foil. When the battery is charged, the zinc metal on the copper foil will be stripped before the cut-off voltage. Thus, one crucial metric to confirm the reversibility and cycle stability of the zinc anode in zinc/copper batteries was the coulomb efficiency (CE) [40]. As shown in Figure 6a, the Zn || Cu battery using pure ZnSO₄ electrolyte maintained a stable CE for 590 cycles, but then the CE value fluctuated and decreased due to the formation of zinc dendrites/by-products or other side reactions. After the [SBP]BF₄ additive was added, the initial cycles of the battery belonged to the remodeling zinc ion coordination stage, so the CE was low. However, the CE value soon reached more than 99% and remained in more than 2200 cycles. These results indicate that the zinc anode can achieve higher cycle stability by using the [SBP]BF₄ + ZnSO₄ electrolyte. At the same time, the voltage–time curves of Zn || Cu batteries were also tested at a constant temperature of 25 °C. As shown in Figure 6b, the substrate metal

(Cu) was used to create a zinc storage cell with a capacity of 2.26 mAh cm^{-2} (Q_t), and a fixed current density of 0.565 mA cm^{-2} was used during the cycle for stripping and electroplating $0.565 \text{ mAh cm}^{-2}$ (Q_c) of Zn. In the final stage, the recoverable capacity Q_s were stripped through the charging process to achieve a specific voltage of 1 V. According to the above conditions, the average CE value was calculated using Equation (1) [41]. The Q_s value of the battery without additives was $1.236 \text{ mAh cm}^{-2}$, and the average CE was calculated to be 87.1%. The Q_s value of the battery with additives was $1.7932 \text{ mAh cm}^{-2}$, and the average CE was calculated to be 94.1%. Therefore, it has been established that the reversibility and utilization rate of the zinc anode may be significantly boosted by adding the $[\text{SBP}]BF_4$ additive to the $ZnSO_4$ electrolyte.

$$\text{CE} = \frac{9Q_c + Q_s}{9Q_c + Q_t} \quad (1)$$

$$\sigma = \frac{L}{R_b S} \quad (2)$$

In order to further prove the role of the $[\text{SBP}]BF_4$ additive, we used graphite as the positive and negative electrodes and glass fiber membrane as the diaphragm, assembled graphite || graphite batteries, tested their electrochemical impedance (EIS) curves (shown in Figure 6c,d), and calculated the ionic conductivity of the two electrolytes in glass fiber separators according to the obtained data and Equation (2) [42]. Where L is the thickness of the glass fiber (0.0675 cm), S is the contact area (1 cm^{-2}), and R_b is the resistance value of the glass fiber obtained by testing, the results showed that the ionic conductivity of the separator with $[\text{SBP}]BF_4 + ZnSO_4$ electrolyte was 24.19 mS cm^{-1} , which was higher than that of the separator with the pure $ZnSO_4$ electrolyte (12.38 mS cm^{-1}). High ionic conductivity of the glass fiber separator can improve the diffusion efficiency of Zn^{2+} , so these data can also help explain the effect of additives on facilitating uniform deposition of zinc ions.

$$t_{Zn^{2+}} = \frac{I_s(\Delta V - I_o R_o)}{I_o(\Delta V - I_s R_s)} \quad (3)$$

In the chronoamperometry experiment (Figure 6e,f), the applied voltage was set to 10 mV , denoted as ΔV . The initial current and resistance were represented by I_o and R_o , respectively, while the steady-state current and resistance were represented by I_s and R_s , respectively. For the cell using electrolyte of $22\text{wt\% } ZnSO_4 + 78\text{wt\% } H_2O$, the initial current (I_o) was 0.158 mA , the initial resistance (R_o) was 218Ω , the steady-state current (I_s) was 0.099 mA , and the steady-state resistance (R_s) was 474Ω . Therefore, according to Equation (3) [42], the calculated $t_{Zn^{2+}}$ was 0.415 . In contrast, for the cell using electrolyte of $22\text{wt\% } ZnSO_4 + 1\text{wt\% } [\text{SBP}]BF_4 + 77\text{wt\% } H_2O$, the initial current (I_o) and resistance (R_o) were found to be 7.747 mA and 183Ω , respectively, while the steady-state current (I_s) and resistance (R_s) were 2.485 mA and 250Ω , respectively. Therefore, the $t_{Zn^{2+}}$ calculated by Equation (3) is 0.739 . The result shows that the addition of $[\text{SBP}]BF_4$ can improve the migration rate of zinc ions and promote the uniform distribution of ions so as to help uniform galvanizing.

In this work, two full batteries were assembled using V_2O_5 as the cathode, Zn foil as the anode, and $ZnSO_4$ and $[\text{SBP}]BF_4 + ZnSO_4$ as the electrolyte, respectively. As shown in Figure 7a, the CV curves of both whole cells showed four (two pairs) redox peaks at a scan rate of 1 mV s^{-1} , which linked to the insertion/extraction of protons and Zn^{2+} ions [43]. Remarkably, the voltage difference of the $Zn || [\text{SBP}]BF_4 + ZnSO_4 || V_2O_5$ cell is only 6 mV , while the voltage difference of the $Zn || ZnSO_4 || V_2O_5$ cell is 32 mV . This indicated that the addition of $[\text{SBP}]BF_4$ can alleviate the polarization of the battery and enhance the reversibility, which had a positive effect on preventing the growth of zinc dendrites [44].

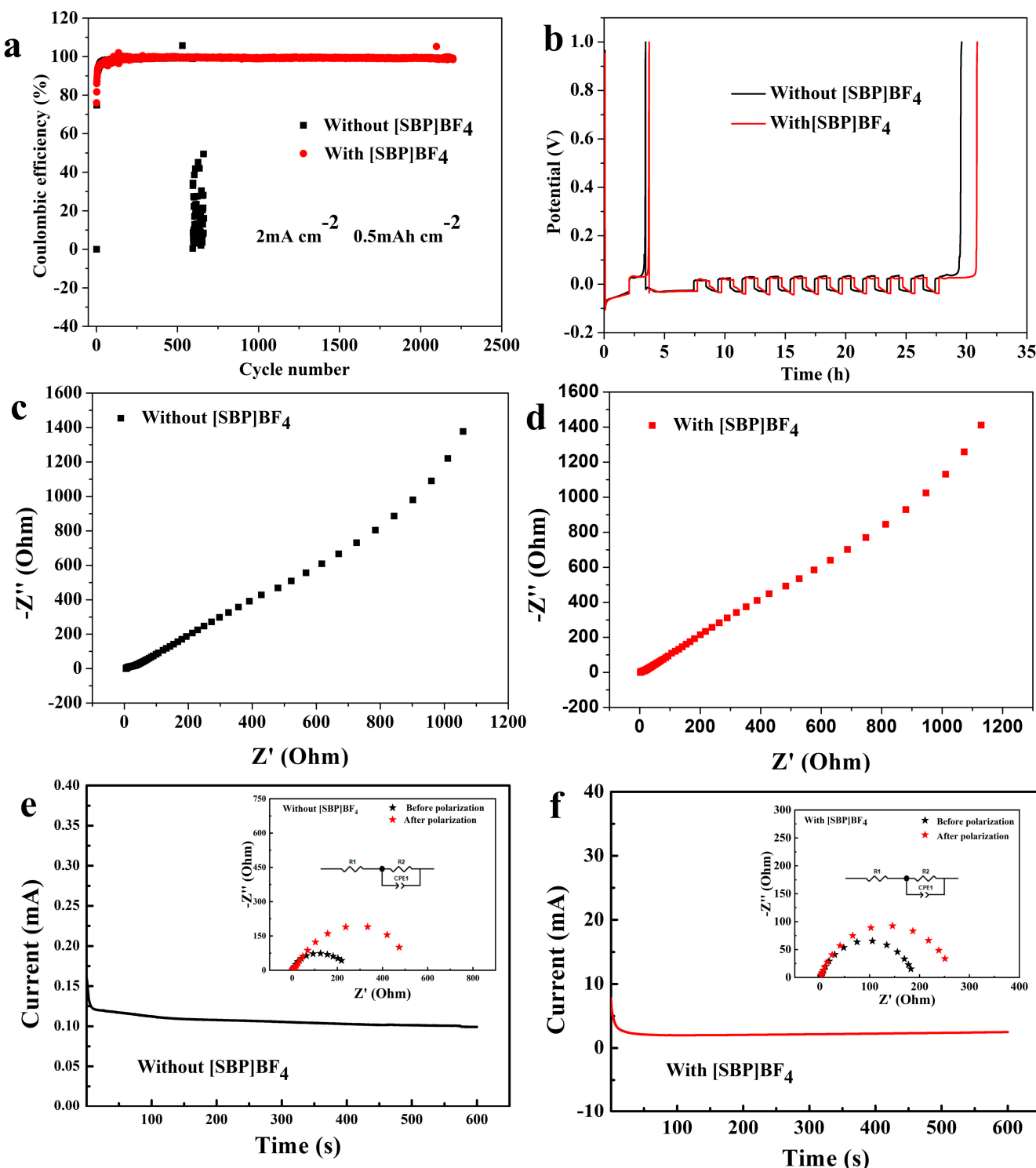


Figure 6. (a) The coulombic efficiency and (b) the voltage–time curves of Zn||Cu batteries using electrolytes with and without additives. Nyquist plots tested of the graphite paper||graphite paper batteries (c) without [SBP]BF₄ additive and (d) with additive in the electrolyte. The chronoamperometry curves of Zn||Zn cells (e) without and (f) with 1wt% [SBP]BF₄ additives in the electrolyte (insets give the corresponding Nyquist plots at initial and steady states after fitting).

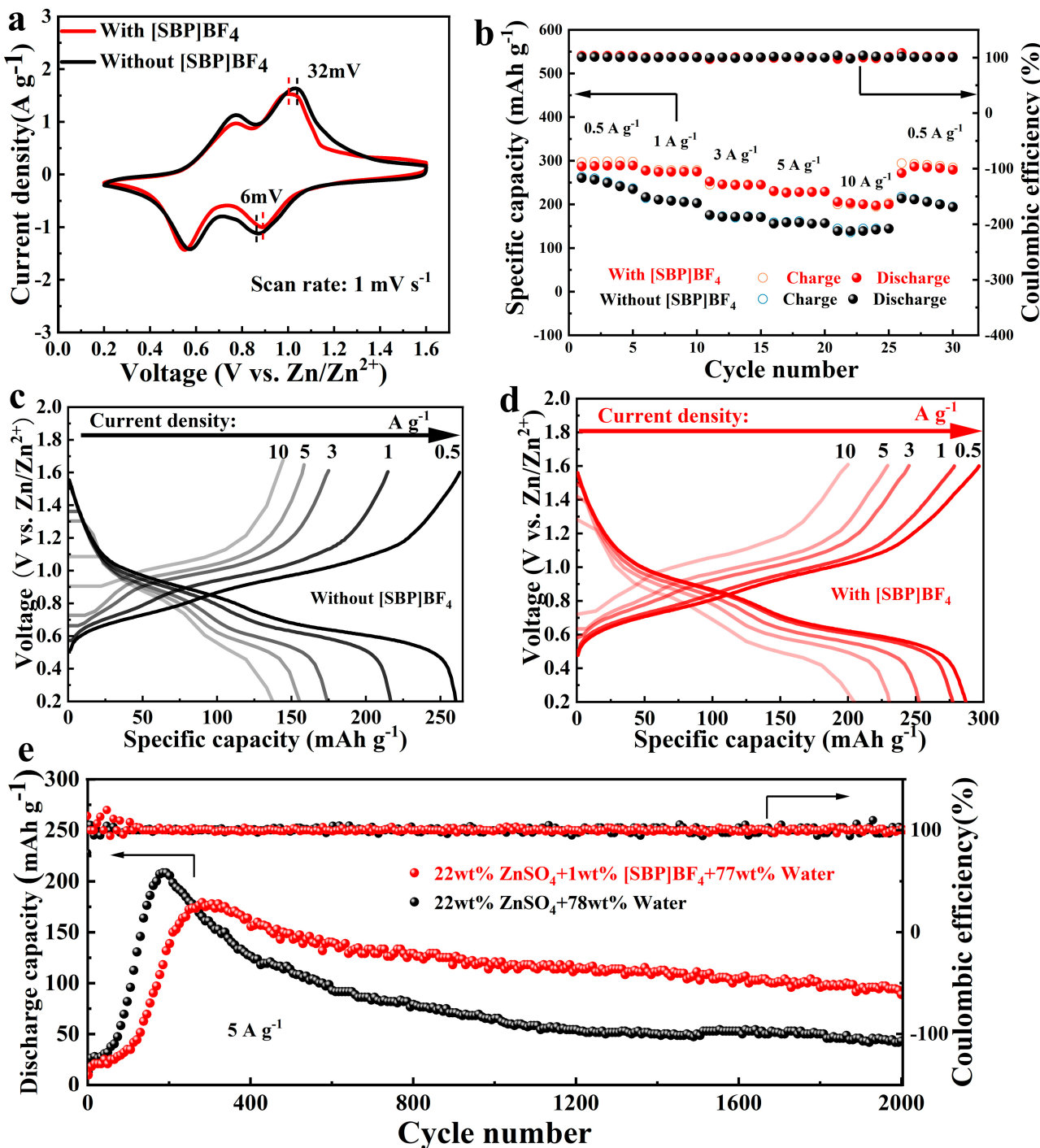


Figure 7. In the study of the electrochemical performance of $\text{Zn} \mid \text{V}_2\text{O}_5$ fuel cells, it was determined that the active material loading on the positive electrode sheet is between 1 and 2 mg cm^{-2} : (a) the CV cures at a scan rate of 1 mV s^{-1} in electrolytes with and without [SBP]BF₄ additives; (b) rate performance in electrolytes with and without [SBP]BF₄ additives; charge/discharge profiles in electrolytes of (c) without and (d) with [SBP]BF₄ additive; (e) cyclic stabilities and efficiencies in electrolytes with and without [SBP]BF₄ additives at 5 A g^{-1} .

Figure 7b displays the rate performance of the two batteries at various current densities (0.5 A g^{-1} , 1 A g^{-1} , 3 A g^{-1} , 5 A g^{-1} , 10 A g^{-1} , and 0.5 A g^{-1}). The discharge specific capacity of the zinc battery with [SBP]BF₄ added to the electrolyte was 296.6 mAh g^{-1} at a current density of 0.5 A g^{-1} , which was higher than that of the battery without the [SBP]BF₄ additive (260.4 mAh g^{-1}). Surprisingly, even at a high current density of

10 A g⁻¹, the battery with the [SBP]BF₄ additive can still maintain a high specific capacity of 166 mAh g⁻¹, which is significantly higher than that of the battery without additives. This revealed that the rate performance of zinc batteries was much enhanced by the addition of additive [SBP]BF₄. Upon evaluating the rate performance, it was noteworthy that the battery's capacity (294.1 mAh g⁻¹) could still be reached when the current density dropped to 0.5 A g⁻¹, indicating strong cycle stability. Figure 7c,d shows the charge/discharge curves of two cells with different current densities, and there are two discharge plateaus near 0.68 and 1.08 V, corresponding to reversible Zn²⁺ insertion and extraction reaction processes, respectively, which are consistent with CV curves. Furthermore, the two batteries' long-term cycle performance was assessed at a current density of 5 A g⁻¹; the outcome is displayed in Figure 7e. Following 2000 cycles, the Zn || [SBP]BF₄ + ZnSO₄ || V₂O₅ cell demonstrates a notable 97 mAh g⁻¹ specific capacity and a high average CE of 99.7%. In contrast, under the same conditions, the specific capacity of the battery without [SBP]BF₄ decreased to 46 mAh g⁻¹, which was majorly attributed to the electrochemical hydrogen evolution corrosion and zinc dendrite growth [45]. The cycling stability of Zn || V₂O₅ batteries, both with and without additives, was evaluated at a current density of 20 A g⁻¹, as depicted in Figure S4. After 3000 cycles, the battery equipped with additives maintained a capacity of 66.7 mAh g⁻¹, outperforming its counterpart devoid of additives, which retained a capacity of merely 33.3 mAh g⁻¹ after the same number of cycles. Following cycling, the zinc foil negative electrode and V₂O₅ positive electrode were detached from the Zn || V₂O₅ battery. Photographic evidence revealed that in the absence of additives (Figure S4a), severe corrosion had occurred on the surface of the zinc foil, leading to the proliferation of zinc dendrites. Consequently, there was an abundance of glass fiber separator residue on the zinc foil's surface. Concurrently, the V₂O₅ positive electrode exhibited significant corrosion accompanied by numerous cracks. In stark contrast, the application of the [SBP]BF₄ additive (Figure S4b) mitigated the corrosion and zinc dendrites on the Zn surface while also enhancing the density and regularity of the V₂O₅ pole piece surface. As shown in Table S1 [35,45–52], we also made a comparison with other electrolyte additives to further illustrate the role of [SBP]BF₄ in inhibiting zinc dendrite formation and corrosion. Therefore, it can be concluded that the introduction of additive [SBP]BF₄ has obvious advantages in improving the rate performance and long-term cycle stability of zinc batteries, and this result provides valuable supporting data for promoting the practical application of zinc-ion batteries.

4. Conclusions

AZIBs exhibit promising potential for use in the domains of portable electronics, electric cars, and large-scale energy storage. However, the metal zinc anode faces problems involving zinc dendrite growth and zinc metal corrosion, as well as anode surface passivation, which affect the electrochemical performance of AZIBs. In order to solve these problems, 1wt% [SBP]BF₄ + 22wt% ZnSO₄ electrolyte was used in this work to improve the stability of the zinc anode. We found that [SBP]BF₄ can preferentially adsorb on the surface of the zinc anode to regulate the uniform nucleation of zinc ions and induce their epitaxial deposition, can improve the solvation sheath of hydrated Zn²⁺ to promote the transport and charge transfer of Zn²⁺, and can produce adaptive SEI film on the surface of the zinc anode to further prevent the occurrence of side reactions between the electrolyte and the electrode. This means that the Zn || Zn battery including the [SBP]BF₄ additive has a cycle life of 2000 h, which was six times longer than the battery lacking [SBP]BF₄. It is worth noting that the Zn || Cu battery with the [SBP]BF₄ additive can also be stably cycled more than 2200 cycles, during which the CE value has been maintained above 99%, proving the good reversibility of the zinc anode. In addition, the Zn || [SBP]BF₄+ZnSO₄ || V₂O₅ full cell has a large specific capacity (288 mAh g⁻¹ at 0.5 A g⁻¹), good rate performance (205 mAh g⁻¹ at 10 A g⁻¹), and a stable long life of 2000 cycles at a current density of 5 A g⁻¹. In summary, the addition of [SBP]BF₄ can increase the rate performance and cycle life of AZIBs in addition to improving the stability and reversibility of the zinc anode.

Supplementary Materials: The following supporting information can be downloaded at: <https://www.mdpi.com/article/10.3390/batteries10030102/s1>.

Author Contributions: Conceptualization, X.Z.; methodology, K.S.; validation, Y.H.; formal analysis, K.X.; investigation, Y.W.; resources, M.H.; data curation, J.L. All authors have read and agreed to the published version of the manuscript.

Funding: This research was funded by the Taishan Scholars Program (NO. tsqnz20230629); the Western Young Scholars Foundations of Chinese Academy of Sciences; the Science Fund of Shandong Laboratory of Yantai Advanced Materials and Green Manufacturing [AMGM2022A02, AMGM2023A04]; the Collaborative Innovation Alliance Fund for Young Science and Technology Worker (HZJJ23-5).

Data Availability Statement: The raw data supporting the conclusions of this article will be made available by the authors on request.

Conflicts of Interest: The authors declare no conflict of interest.

References

1. Chayambuka, K.; Mulder, G.; Danilov, D.L.; Notten, P.H.L. From Li-Ion Batteries toward Na-Ion Chemistries: Challenges and Opportunities. *Adv. Energy Mater.* **2020**, *10*, 2001310. [[CrossRef](#)]
2. Ma, L.; Schroeder, M.A.; Borodin, O.; Pollard, T.P.; Ding, M.S.; Wang, C.; Xu, K. Realizing High Zinc Reversibility in Rechargeable Batteries. *Nat. Energy* **2020**, *5*, 743–749. [[CrossRef](#)]
3. Raza, H.; Cheng, J.; Lin, C.; Majumder, S.; Zheng, G.; Chen, G. High-Entropy Stabilized Oxides Derived via a Low-Temperature Template Route for High-Performance Lithium-Sulfur Batteries. *EcoMat* **2023**, *5*, e12324. [[CrossRef](#)]
4. Wang, H.; Zhou, A.; Hu, X.; Hu, Z.; Zhang, F.; Huang, Y.; Li, L.; Wu, F.; Chen, R. Bifunctional Dynamic Adaptive Interphase Reconfiguration for Zinc Deposition Modulation and Side Reaction Suppression in Aqueous Zinc Ion Batteries. *ACS Nano* **2023**, *17*, 11946–11956. [[CrossRef](#)]
5. Zhou, T.; Xie, L.; Han, Q.; Qiu, X.; Xiao, Y.; Yang, X.; Liu, X.; Yang, S.; Zhu, L.; Cao, X. Progress and Prospect of Vanadates as Aqueous Zn-Ion Batteries Cathodes. *Coord. Chem. Rev.* **2024**, *498*, 215461. [[CrossRef](#)]
6. Deng, W.; Xu, Z.; Wang, X. High-Donor Electrolyte Additive Enabling Stable Aqueous Zinc-Ion Batteries. *Energy Storage Mater.* **2022**, *52*, 52–60. [[CrossRef](#)]
7. Deng, R.; He, Z.; Chu, F.; Lei, J.; Cheng, Y.; Zhou, Y.; Wu, F. An Aqueous Electrolyte Densified by Perovskite SrTiO₃ Enabling High-Voltage Zinc-Ion Batteries. *Nat. Commun.* **2023**, *14*, 4981. [[CrossRef](#)] [[PubMed](#)]
8. Kuai, X.; Li, K.; Chen, J.; Wang, H.; Yao, J.; Chiang, C.-L.; Liu, T.; Ye, H.; Zhao, J.; Lin, Y.-G.; et al. Interfacial Engineered Vanadium Oxide Nanoheterostructures Synchronizing High-Energy and Long-Term Potassium-Ion Storage. *ACS Nano* **2022**, *16*, 1502–1510. [[CrossRef](#)] [[PubMed](#)]
9. Xu, X.; Zhu, X.; Li, S.; Xu, Y.; Sun, L.; Shi, L.; Song, M. In Situ Constructing Solid Electrolyte Interphase and Optimizing Solvation Shell for a Stable Zn Anode. *J. Electron. Mater.* **2024**, *53*, 288–297. [[CrossRef](#)]
10. Shi, X.; Wang, J.; Yang, F.; Liu, X.; Yu, Y.; Lu, X. Metallic Zinc Anode Working at 50 and 50 mAh cm⁻² with High Depth of Discharge via Electrical Double Layer Reconstruction. *Adv. Funct. Mater.* **2023**, *33*, 2211917. [[CrossRef](#)]
11. Jia, X.; Liu, C.; Neale, Z.G.; Yang, J.; Cao, G. Active Materials for Aqueous Zinc Ion Batteries: Synthesis, Crystal Structure, Morphology, and Electrochemistry. *Chem. Rev.* **2020**, *120*, 7795–7866. [[CrossRef](#)]
12. Wang, M.; Wu, X.; Yang, D.; Zhao, H.; He, L.; Su, J.; Zhang, X.; Yin, X.; Zhao, K.; Wang, Y.; et al. A Colloidal Aqueous Electrolyte Modulated by Oleic Acid for Durable Zinc Metal Anode. *Chem. Eng. J.* **2023**, *451*, 138589. [[CrossRef](#)]
13. Jia, H.; Wang, Z.; Tawiah, B.; Wang, Y.; Chan, C.-Y.; Fei, B.; Pan, F. Recent Advances in Zinc Anodes for High-Performance Aqueous Zn-Ion Batteries. *Nano Energy* **2020**, *70*, 104523. [[CrossRef](#)]
14. Raza, H.; Bai, S.; Cheng, J.; Majumder, S.; Zhu, H.; Liu, Q.; Zheng, G.; Li, X.; Chen, G. Li-S Batteries: Challenges, Achievements and Opportunities. *Electrochim. Energy Rev.* **2023**, *6*, 29. [[CrossRef](#)]
15. Chao, D.; Zhou, W.; Xie, F.; Ye, C.; Li, H.; Jaroniec, M.; Qiao, S.-Z. Roadmap for Advanced Aqueous Batteries: From Design of Materials to Applications. *Sci. Adv.* **2020**, *6*, eaba4098. [[CrossRef](#)] [[PubMed](#)]
16. Zhang, X.; Jia, C.; Zhang, J.; Zhang, L.; Liu, X. Smart Aqueous Zinc Ion Battery: Operation Principles and Design Strategy. *Adv. Sci.* **2024**, *11*, 2305201. [[CrossRef](#)] [[PubMed](#)]
17. Yoo, G.; Lee, Y.-G.; Im, B.; Kim, D.G.; Jo, Y.-R.; An, G. Integrated Solution for a Stable and High-Performance Zinc-Ion Battery Using an Electrolyte Additive. *Energy Storage Mater.* **2023**, *61*, 102845. [[CrossRef](#)]
18. Fang, T.; Liu, Q.; Hu, A.; Meng, J.; Fu, Y.; Shi, Z. Dendrite-Free and Stable Zinc-Ion Batteries Enabled by a Cation-Anion Synergistic Regulation Additive. *J. Power Sources* **2023**, *581*, 233521. [[CrossRef](#)]
19. Yin, J.; Li, M.; Feng, X.; Cui, T.; Chen, J.; Li, F.; Wang, M.; Cheng, Y.; Ding, S.; Xu, X.; et al. Unveiling the Multifunctional Regulation Effect of a Glutamine Additive for Highly Reversible Zn Metal Anodes. *J. Mater. Chem. A* **2024**, *12*, 1543–1550. [[CrossRef](#)]
20. Abdulla, J.; Cao, J.; Zhang, D.; Zhang, X.; Sriprachuabwong, C.; Kheawhom, S.; Wangyao, P.; Qin, J. Elimination of Zinc Dendrites by Graphene Oxide Electrolyte Additive for Zinc-Ion Batteries. *ACS Appl. Energ. Mater.* **2021**, *4*, 4602–4609. [[CrossRef](#)]

21. Lin, Y.; Mai, Z.; Liang, H.; Li, Y.; Yang, G.; Wang, C. Dendrite-Free Zn Anode Enabled by Anionic Surfactant-Induced Horizontal Growth for Highly-Stable Aqueous Zn-Ion Pouch Cells. *Energy Environ. Sci.* **2023**, *16*, 687–697. [[CrossRef](#)]
22. Su, K.; Chen, J.; Zhang, X.; Feng, J.; Xu, Y.; Pu, Y.; Wang, C.; Ma, P.; Wang, Y.; Lang, J. Inhibition of Zinc Dendrites by Dopamine Modified Hexagonal Boron Nitride Electrolyte Additive for Zinc-Ion Batteries. *J. Power Sources* **2022**, *548*, 232074. [[CrossRef](#)]
23. Wei, T.; Zhang, X.; Ren, Y.; Wang, Y.; Li, Z.; Zhang, H.; Hu, L. Reconstructing Anode/Electrolyte Interface and Solvation Structure towards High Stable Zinc Anode. *Chem. Eng. J.* **2023**, *457*, 141272. [[CrossRef](#)]
24. Xu, M.; Ivey, D.G.; Qu, W.; Xie, Z. Study of the Mechanism for Electrodeposition of Dendrite-Free Zinc in an Alkaline Electrolyte Modified with 1-Ethyl-3-Methylimidazolium Dicyanamide. *J. Power Sources* **2015**, *274*, 1249–1253. [[CrossRef](#)]
25. Bayer, M.; Overhoff, G.M.; Gui, A.L.; Winter, M.; Bieker, P.; Schulze, S. Influence of Water Content on the Surface Morphology of Zinc Deposited from EMImOTf/Water Mixtures. *J. Electrochem. Soc.* **2019**, *166*, A909–A914. [[CrossRef](#)]
26. Ma, Z.; Kan, J. Study of Cylindrical Zn/PANI Secondary Batteries with the Electrolyte Containing Alkylimidazolium Ionic Liquid. *Synth. Met.* **2013**, *174*, 58–62. [[CrossRef](#)]
27. Lahiri, A.; Yang, L.; Li, G.; Endres, F. Mechanism of Zn-Ion Intercalation/Deintercalation in a Zn-Polypyrrole Secondary Battery in Aqueous and Bio-Ionic Liquid Electrolytes. *ACS Appl. Mater. Interfaces* **2019**, *11*, 45098–45107. [[CrossRef](#)] [[PubMed](#)]
28. Cao, L.; Li, D.; Pollard, T.; Deng, T.; Zhang, B.; Yang, C.; Chen, L.; Vatamanu, J.; Hu, E.; Hourwitz, M.J.; et al. Fluorinated Interphase Enables Reversible Aqueous Zinc Battery Chemistries. *Nat. Nanotechnol.* **2021**, *16*, 902–910. [[CrossRef](#)]
29. Liu, Z.; El Abedin, S.Z.; Endres, F. Electrodeposition of Zinc Films from Ionic Liquids and Ionic Liquid/Water Mixtures. *Electrochim. Acta* **2013**, *89*, 635–643. [[CrossRef](#)]
30. Wang, R.; Fang, C.; Yang, L.; Li, K.; Zhu, K.; Liu, G.; Chen, J. The Novel Ionic Liquid and Its Related Self-Assembly in the Areas of Energy Storage and Conversion. *Small Sci.* **2022**, *2*, 2200048. [[CrossRef](#)]
31. Lebedeva, O.; Kultin, D.; Kustov, L. Advanced Research and Prospects on Polymer Ionic Liquids: Trends, Potential and Application. *Green Chem.* **2023**, *25*, 9001–9019. [[CrossRef](#)]
32. Zhao, P.; Yang, B.; Chen, J.; Lang, J.; Zhang, T.; Yan, X. A Safe, High-Performance, and Long-Cycle Life Zinc-Ion Hybrid Capacitor Based on Three-Dimensional Porous Activated Carbon. *Acta Phys.-Chim. Sin.* **2020**, *36*, 1904050. [[CrossRef](#)]
33. Huo, H.; Li, X.; Chen, Y.; Liang, J.; Deng, S.; Gao, X.; Doyle-Davis, K.; Li, R.; Guo, X.; Shen, Y.; et al. Bifunctional Composite Separator with a Solid-State-Battery Strategy for Dendrite-Free Lithium Metal Batteries. *Energy Storage Mater.* **2020**, *29*, 361–366. [[CrossRef](#)]
34. Chen, R.; Zhang, W.; Huang, Q.; Guan, C.; Zong, W.; Dai, Y.; Du, Z.; Zhang, Z.; Li, J.; Guo, F.; et al. Trace Amounts of Triple-Functional Additives Enable Reversible Aqueous Zinc-Ion Batteries from a Comprehensive Perspective. *Nano-Micro Lett.* **2023**, *15*, 81. [[CrossRef](#)]
35. Chen, J.; Zhou, W.; Quan, Y.; Liu, B.; Yang, M.; Chen, M.; Han, X.; Xu, X.; Zhang, P.; Shi, S. Ionic Liquid Additive Enabling Anti-Freezing Aqueous Electrolyte and Dendrite-Free Zn Metal Electrode with Organic/Inorganic Hybrid Solid Electrolyte Interphase Layer. *Energy Storage Mater.* **2022**, *53*, 629–637. [[CrossRef](#)]
36. Chen, X.; Liu, T.; Ding, Y.; Sun, X.; Huang, J.; Qiao, J.; Peng, S. Controlled Nucleation and Growth for the Dendrite-Free Zinc Anode in Aqueous Zinc-Ion Battery. *J. Alloys Compd.* **2024**, *970*, 172584. [[CrossRef](#)]
37. Chen, R.; Liu, Q.; Xu, L.; Zuo, X.; Liu, F.; Zhang, J.; Zhou, X.; Mai, L. Zwitterionic Bifunctional Layer for Reversible Zn Anode. *ACS Energy Lett.* **2022**, *7*, 1719–1727. [[CrossRef](#)]
38. Zheng, S.; Wei, L.; Zhang, Z.; Pan, J.; He, J.; Gao, L.; Li, C.C. In Situ Polymerization of Ionic Liquid with Tunable Phase Separation for Highly Reversible and Ultralong Cycle Life Zn-Ion Battery. *Nano Lett.* **2022**, *22*, 9062–9070. [[CrossRef](#)] [[PubMed](#)]
39. Jang, J.; Jae-Sun, S.; Ko, S.; Park, H.; Song, W.-J.; Park, C.B.; Kang, J. Self-Assembled Protective Layer by Symmetric Ionic Liquid for Long-Cycling Lithium-Metal Batteries. *Adv. Energy Mater.* **2022**, *12*, 2103955. [[CrossRef](#)]
40. Gou, Q.; Luo, H.; Zhang, Q.; Deng, J.; Zhao, R.; Odunmbaku, O.; Wang, L.; Li, L.; Zheng, Y.; Li, J.; et al. Electrolyte Regulation of Bio-Inspired Zincophilic Additive toward High-Performance Dendrite-Free Aqueous Zinc-Ion Batteries. *Small* **2023**, *19*, 2207502. [[CrossRef](#)] [[PubMed](#)]
41. Ma, L.; Schroeder, M.A.; Pollard, T.P.; Borodin, O.; Ding, M.S.; Sun, R.; Cao, L.; Ho, J.; Baker, D.R.; Wang, C.; et al. Critical Factors Dictating Reversibility of the Zinc Metal Anode. *Energy Environ. Mater.* **2020**, *3*, 516–521. [[CrossRef](#)]
42. Hao, J.; Li, X.; Zhang, S.; Yang, F.; Zeng, X.; Zhang, S.; Bo, G.; Wang, C.; Guo, Z. Designing Dendrite-Free Zinc Anodes for Advanced Aqueous Zinc Batteries. *Adv. Funct. Mater.* **2020**, *30*, 2001263. [[CrossRef](#)]
43. Li, B.; Xue, J.; Lv, X.; Zhang, R.; Ma, K.; Wu, X.; Dai, L.; Wang, L.; He, Z. A Facile Coating Strategy for High Stability Aqueous Zinc Ion Batteries: Porous Rutile Nano-TiO₂ Coating on Zinc Anode. *Surf. Coat. Technol.* **2021**, *421*, 127367. [[CrossRef](#)]
44. Yong, B.; Ma, D.; Wang, Y.; Mi, H.; He, C.; Zhang, P. Understanding the Design Principles of Advanced Aqueous Zinc-Ion Battery Cathodes: From Transport Kinetics to Structural Engineering, and Future Perspectives. *Adv. Energy Mater.* **2020**, *10*, 2002354. [[CrossRef](#)]
45. Xu, J.; Wang, M.; Asraful Alam, M.; Hoang, T.K.A.; Zhang, Y.; Li, H.; Lv, Y.; Zhao, A.; Xiong, W. Employing Cationic Kraft Lignin as Electrolyte Additive to Enhance the Electrochemical Performance of Rechargeable Aqueous Zinc-Ion Battery. *Fuel* **2023**, *333*, 126450. [[CrossRef](#)]
46. Sun, P.; Ma, L.; Zhou, W.; Qiu, M.; Wang, Z.; Chao, D.; Mai, W. Simultaneous Regulation on Solvation Shell and Electrode Interface for Dendrite-Free Zn Ion Batteries Achieved by a Low-Cost Glucose Additive. *Angew. Chem. Int. Ed.* **2021**, *60*, 18247–18255. [[CrossRef](#)]

47. Zou, P.; Lin, R.; Pollard, T.P.; Yao, L.; Hu, E.; Zhang, R.; He, Y.; Wang, C.; West, W.C.; Ma, L.; et al. Localized Hydrophobicity in Aqueous Zinc Electrolytes Improves Zinc Metal Reversibility. *Nano Lett.* **2022**, *22*, 7535–7544. [[CrossRef](#)] [[PubMed](#)]
48. Zhang, Q.; Luan, J.; Fu, L.; Wu, S.; Tang, Y.; Ji, X.; Wang, H. The Three-Dimensional Dendrite-Free Zinc Anode on a Copper Mesh with a Zinc-Oriented Polyacrylamide Electrolyte Additive. *Angew. Chem. Int. Ed.* **2019**, *58*, 15841–15847. [[CrossRef](#)]
49. Zhang, Q.; Ma, Y.; Lu, Y.; Zhou, X.; Lin, L.; Li, L.; Yan, Z.; Zhao, Q.; Zhang, K.; Chen, J. Designing Anion-Type Water-Free Zn²⁺ Solvation Structure for Robust Zn Metal Anode. *Angew. Chem. Int. Ed.* **2021**, *60*, 23357–23364. [[CrossRef](#)] [[PubMed](#)]
50. Cui, J.; Liu, X.; Xie, Y.; Wu, K.; Wang, Y.; Liu, Y.; Zhang, J.; Yi, J.; Xia, Y. Improved Electrochemical Reversibility of Zn Plating/Stripping: A Promising Approach to Suppress Water-Induced Issues through the Formation of H-Bonding. *Mater. Today Energy* **2020**, *18*, 100563. [[CrossRef](#)]
51. Hao, J.; Long, J.; Li, B.; Li, X.; Zhang, S.; Yang, F.; Zeng, X.; Yang, Z.; Pang, W.K.; Guo, Z. Toward High-Performance Hybrid Zn-Based Batteries via Deeply Understanding Their Mechanism and Using Electrolyte Additive. *Adv. Funct. Mater.* **2019**, *29*, 1903605. [[CrossRef](#)]
52. Zeng, X.; Mao, J.; Hao, J.; Liu, J.; Liu, S.; Wang, Z.; Wang, Y.; Zhang, S.; Zheng, T.; Liu, J.; et al. Electrolyte Design for In Situ Construction of Highly Zn²⁺-Conductive Solid Electrolyte Interphase to Enable High-Performance Aqueous Zn-Ion Batteries under Practical Conditions. *Adv. Mater.* **2021**, *33*, 2007416. [[CrossRef](#)]

Disclaimer/Publisher's Note: The statements, opinions and data contained in all publications are solely those of the individual author(s) and contributor(s) and not of MDPI and/or the editor(s). MDPI and/or the editor(s) disclaim responsibility for any injury to people or property resulting from any ideas, methods, instructions or products referred to in the content.